Available online at www.sciencedirect.com
ScienceDirect
International Journal of Mechanical Sciences 50 (2008) 233–246
International Journal of Mechanical Sciences
www.elsevier.com/locate/ijmecsci

The collapse response of sandwich beams with a Y-frame core subjected to distributed and local loading

V. Rubino, V.S. Deshpande*, N.A. Fleck

Engineering Department, Cambridge University, Trumpington Street, Cambridge, CB2 1PZ, UK

Received 12 November 2006; received in revised form 23 June 2007; accepted 4 July 2007
Available online 25 July 2007

Abstract

Sandwich beams comprising a Y-frame core have been manufactured by assembling and brazing together pre-folded sheets made from AISI type 304 stainless steel. The collapse responses of the Y-frame core have been measured in out-of-plane compression, longitudinal shear and transverse shear; and the measurements have been compared with finite element predictions. Experiments and calculations both indicate that the compressive response is governed by bending of the constituent struts of the Y-frame and is sensitive to the choice of lateral boundary conditions: the energy absorption for a no-sliding boundary condition exceeds that for free-sliding. Under longitudinal shear, the leg of the Y-frame undergoes uniform shear prior to the onset of plastic buckling. Consequently, the longitudinal shear strength of the Y-frame much exceeds its compressive strength and transverse shear strength. Sandwich beams were also indented by a flat bottomed punch, and a relatively high indentation strength was observed. It is argued that this is due to the high longitudinal shear strength of the Y-frame. While finite element calculations capture the measurements to reasonable accuracy, a simple analytical model over-predicts the indentation strength. Finally, the finite element method was used to investigate the energy absorption capacity of the sandwich beams under indentation loading. The calculations reveal that for a given tensile failure strain of the face-sheet material, a sandwich beam with Y-frame core has a comparable performance to that of a sandwich beam with a metal foam core. The relative performance is, however, sensitive to the choice of design parameter: when the indentation depth is taken as the design constraint, the sandwich beam with a Y-frame core outperforms the sandwich beam with the metal foam core.

Keywords: Sandwich beams; Energy absorption; Y-frame core; Indentation

1. Introduction

Commercial and military ship structures require adequate strength to survive impact by submerged rocks, icebergs and collisions with other vessels. Current designs are based upon either a monolithic skin with an internal stiffening and strengthening frame or upon double-hulled designs which have minimal mechanical coupling between the inner and outer hulls. There is current industrial interest in determining whether significant enhancements in structural stiffness, strength and energy absorption with no weight penalty can be achieved by employing sandwich construction.

Over the past few years, a set of lattice materials have been devised for sandwich cores. The nodal connectivity of these lattices is sufficiently high for them to deform by the axial stretching of the constituent members under all loading states, see for example Deshpande and Fleck [1]. Consequently, these materials have a higher specific stiffness and strength than metallic foams which deform by cell-wall bending. The best choice of core remains unclear for hulls designed primarily to withstand low velocity collision: weaker sandwich cores diffuse an external transverse load over a larger portion of the hull and may thereby absorb more energy prior to hull perforation.

Over the past decade or so there have been substantial changes in ship design, see for example the review by Paik [2]. In the current study, we measure and analyse the performance of the Y-shaped sandwich core, as proposed

*Corresponding author. Fax: +44 1223 332662.
E-mail address: vsd@eng.cam.ac.uk (V.S. Deshpande).

0020-7403/$ - see front matter © 2007 Elsevier Ltd. All rights reserved.
doi:10.1016/j.ijmecsci.2007.07.007

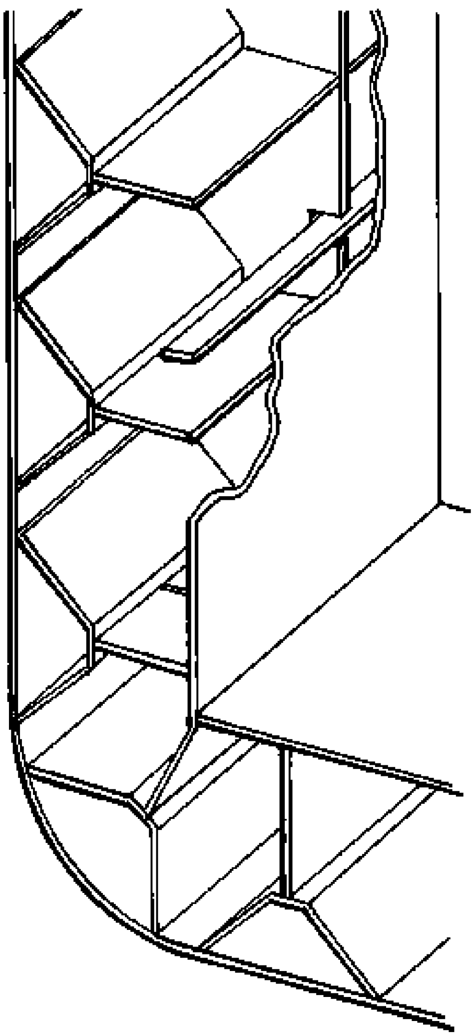

Fig. 1. Sketch of the Y-frame sandwich core as used in ship hull construction. The core is sandwiched between the outer and inner hull of the ship.

by Schelde Shipbuilding.[1] It is manufactured by conventional welding methods of steel sheets and its topology is shown in Fig. 1. Full-scale ship collision trials reveal that the Y-frame design is more resistant to tearing than conventional monolithic designs, see Wevers and Vredeveldt [3] and Ludolphy [4]. Likewise, the finite element simulations by Konter et al. [5] suggest that the Y-frame confers improved perforation resistance. Naar et al. [6] have argued in broad terms that the ability of the bending-governed Y-frame topology to spread the impact load over a wide area, combined with the in-plane high stretching resistance of the Y-frame, gives the enhanced performance of the Y-frame sandwich construction over conventional single and double hull designs. However, a detailed analysis of the elastic–plastic indentation behaviour of the Y-frame sandwich beam has been lacking to date.

[1]Royal Schelde, P.O. Box 16 4380, AA Vlissingen, The Netherlands.

Pedersen et al. [7] performed a finite element investigation of the compressive response of the Y-frame. They developed maps of the compressive strength and energy absorption of the Y-frame with the geometric parameters of the Y-frame as axes of these maps. Their study revealed that the compressive collapse response of the Y-frame is sensitive to the size of the web and to the choice of boundary conditions. No experimental investigations into the effective properties of the Y-frame and into the indentation response of Y-frame core sandwich beams have been reported to date. This is the principal aim of the current study.

1.1. Scope of study

A combined experimental, finite element and analytical investigation is presented on the indentation response of Y-frame sandwich beams. First, the manufacturing procedure for laboratory scale Y-frame sandwich beams is described and measurements are given for the compressive and shear responses of the Y-frame core. These measurements are compared with 3D finite element simulations. Next, the measured indentation response of Y-frame sandwich beams is reported. Analytical and finite element predictions are developed and compared with these experimental values. Additional finite element calculations on the indentation response of sandwich beams with isotropic foam cores are used to identify those properties of the core that enhance energy absorption of the sandwich beams prior to perforation of the face-sheets. Finally, the sensitivity of energy absorption to the ductility of the face-sheets is explored.

2. Specimen manufacture

Scaled-down (approximately 1/10 scale) Y-frame sandwich cores of depth $c = 44\,\text{mm}$ were manufactured from AISI 304 stainless steel sheets of thickness $g = 0.5\,\text{mm}$. The cross-sectional dimensions of the Y-frame are given in Fig. 2a. A global co-ordinate reference frame is included in the figure in order to clarify the various loading directions used in the mechanical tests: x_1 is the longitudinal axis of the Y-frame, x_2 denotes the transverse direction and x_3 is the out-of-plane direction for the sandwich beam. The Y-frames are close-packed along the x_2 direction such that adjacent Y-frames touch; the relative density of the as-manufactured Y-frame sandwich core (that is, the ratio of effective density of the smeared-out core to that of the parent solid material) is 2.1%.

Y-frame sandwich beams of length $L = 600\,\text{mm}$ were manufactured as follows. The stainless steel sheets were computer-numerical-control (CNC) folded to form the upper part of the Y-frame and the Y-frame leg. Slots were then CNC-cut into the Y-frame web and the Y-frame leg was fitted into the upper part of the Y-frame, as sketched in Fig. 2b. The assembly was then spot welded to face-sheets of thickness $t = 0.6$ or $1.2\,\text{mm}$. The braze alloy Ni–Cr 25-P10 (wt%) was applied uniformly over all sheets of the

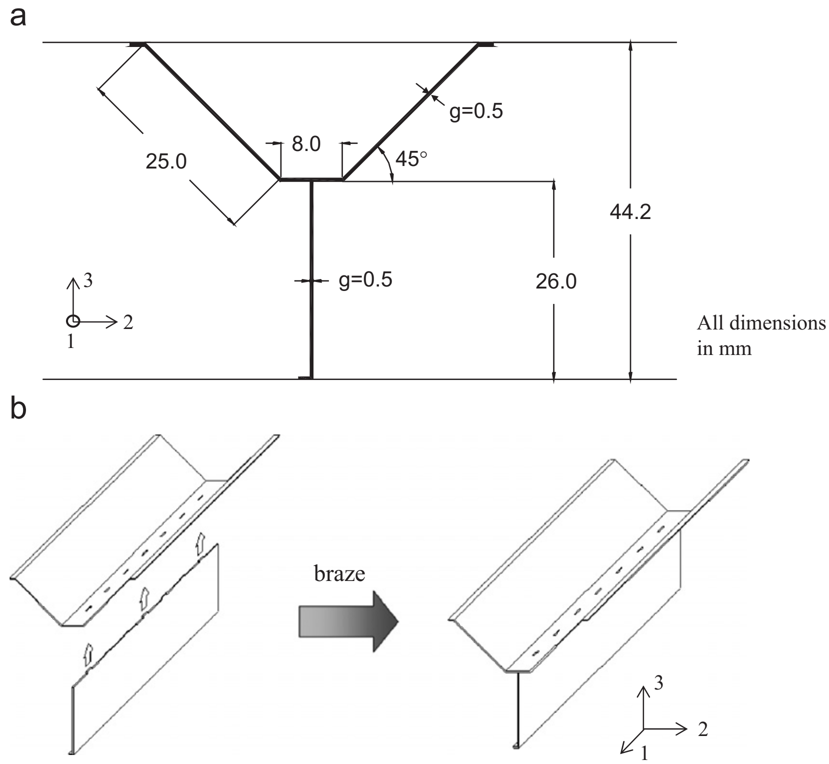

Fig. 2. (a) Geometry of the Y-frame sandwich core used in this study. (b) Sketch of the manufacturing route for the scaled-down Y-frame sandwich core.

assembly and the assembly was brazed together in a vacuum furnace at 1075 °C in a dry argon atmosphere at 0.03–0.1 mbar. Finally, the beams were water-jet cut to the required length.

Tensile specimens of dog-bone geometry were cut from the as-received 304 stainless steel sheets and were subjected to the same brazing cycle as that used to manufacture the Y-frame beam specimens. The measured true tensile stress versus logarithmic strain response at a strain rate of $\dot{\varepsilon} = 10^{-4}\,s^{-1}$ is shown in Fig. 3. The stainless steel behaves in an elastic–plastic manner with a Young's modulus $E = 210\,GPa$, a yield strength of $\sigma_Y = 210\,MPa$ and linear hardening in the plastic regime with a tangent modulus of $E_t \approx 2.1\,GPa$.

3. Compressive and shear responses of the Y-frame sandwich core

Two types of tests were conducted on the Y-frame sandwich core: (a) out-of-plane compression, and (b) shear in the transverse and longitudinal directions. These loading directions are of principal practical interest for a Y-framed sandwich plate. The sandwich core is treated as a homogeneous effective medium and its stress versus strain behaviour is measured.

3.1. Compressive response

The σ_{33} versus ε_{33} out-of-plane compressive response of Y-frame sandwich specimens, of length $L = 140\,mm$, was investigated for the following two sets of lateral boundary condition (see Fig. 4):

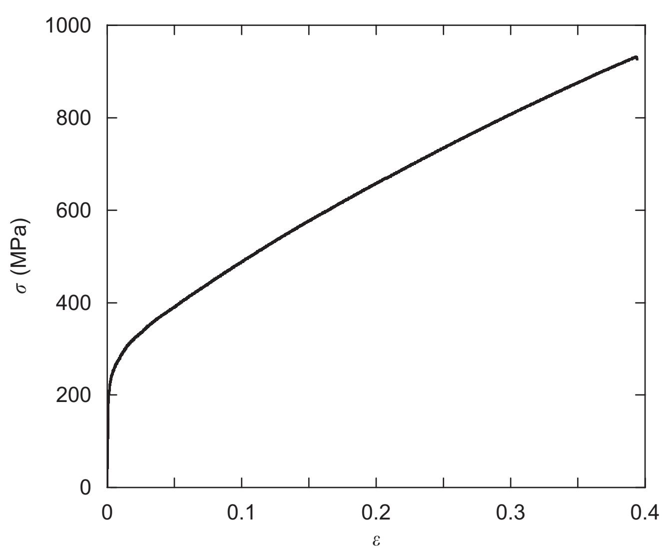

Fig. 3. The quasi-static tensile stress versus strain response of the as-brazed 304 stainless steel as used to manufacture the Y-frame sandwich beams.

(a) *no-sliding*. The face-sheets of the Y-frame were clamped to the platens of the test machine. Consequently, the face-sheets were prevented from relative sliding.
(b) *free-sliding*. One face-sheet was clamped to the stationary platen of the test machine while linear bearings were

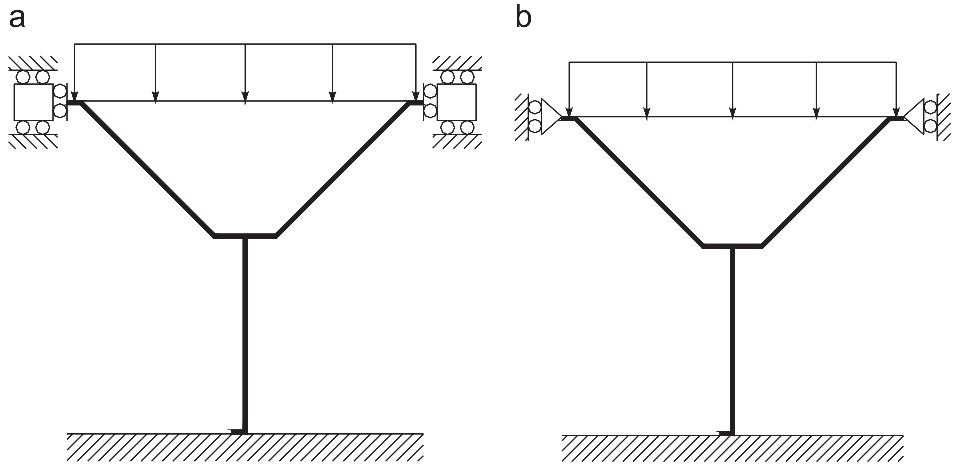

Fig. 4. Sketches of a unit cell of the Y-frame sandwich core with the two types of uniaxial compression boundary conditions considered. (a) The free-sliding and (b) no-sliding boundary conditions.

located between the other face-sheet and the moving platen of the test machine. Consequently, the face-sheets of the Y-frame sandwich could slide past each other during the uniaxial compression test.

In both sets of experiments, the Y-frame core was brazed to 0.6 mm thick 304 stainless steel face-sheets. These face-sheets remained elastic during the tests and so the measured compressive response of the Y-frame core is independent of the face-sheet properties.

These two sets of boundary conditions represent the limiting cases where the supports either (a) completely restrict or (b) permit free-sliding of the outer face of the ship hull with respect to the inner hull. These choices are appropriate for large structures comprising many Y-shaped webs and subjected to uniform macroscopic loading. Other boundary conditions, permitting relative rotation of the two faces of the Y-frame sandwich beams, are also of practical relevance but are beyond the scope of the present investigation.

The compression experiments were performed using a screw-driven testing machine at a nominal compressive strain rate of approximately $\dot{\varepsilon}_{33} = 10^{-4}\,\mathrm{s}^{-1}$. The load was measured by the load cell of the test machine and was used to define the nominal compressive stress σ_{33}, while a laser extensometer measured the relative approach of the face-sheets of the Y-frame sandwich and thereby gave the applied nominal compressive strain ε_{33}. The measured nominal compressive stress versus strain responses of the Y-frame sandwich cores are plotted in Fig. 5a and b for the no-sliding and free-sliding boundary conditions, respectively. The response of the Y-frame core for both boundary conditions is characterized by an initial elastic stress response, a peak stress and subsequent softening. The peak stress of $\sigma_{33}^{p} = 0.54\,\mathrm{MPa}$ for no-sliding is higher than the peak stress of $\sigma_{33}^{p} = 0.40\,\mathrm{MPa}$ for the free-sliding boundary condition. A montage of photographs of the Y-frame specimens at selected levels of applied compressive strain are shown in Figs. 6a and 7a for the no-sliding and free-sliding cases, respectively. These photographs show that the deformation modes differ: while plastic deformation spreads over the entire Y-frame in the no-sliding case, the upper half of the Y-frame remains elastic in the free-sliding case.

3.2. Shear response

The transverse shear ($\tau_{23}-\gamma_{23}$) and longitudinal shear ($\tau_{13}-\gamma_{13}$) responses of the Y-frame sandwich cores were measured using a double-lap shear apparatus as shown in Fig. 8. Each shear specimen comprised two nominally identical sandwich beams bolted to the platens of the double-lap shear apparatus. Pin-grips were used to fasten the shear rig to the test machine. This arrangement provided an indeterminate constraint on the deformation of the specimen in the x_3 direction: the constraint is intermediate between that of zero load and zero displacement in the x_3 direction. The load cell of the test machine was used to measure the load and a laser extensometer measured the relative displacement of the platens in order to infer the applied shear strain.

3.2.1. Longitudinal shear tests

The measured longitudinal shear response ($\tau_{13}-\gamma_{13}$) of the Y-frame sandwich core with aspect ratio $L/c \approx 7$ ($L = 300\,\mathrm{mm}$) is plotted in Fig. 9. Two separate measurements are plotted to give an indication of the scatter in the experimental results. The Y-frame sandwich core displays an initial elastic response followed by an almost ideally plastic stress versus strain history with a peak shear strength $\tau_{13}^{p} \approx 1.7\,\mathrm{MPa}$. A photograph of the Y-frame at a strain level of $\gamma_{13} = 0.1$ is included in Fig. 10a. The photograph shows that wrinkling occurs in the leg of the Y-frame with negligible deformation of the upper half of the Y-frame. Tearing initiates at the joint between face-sheet and leg at $\gamma_{13} \approx 0.05$.

The wrinkling deformation mode of the Y-frame leg in Fig. 10a is expected to be sensitive to end effects and thus

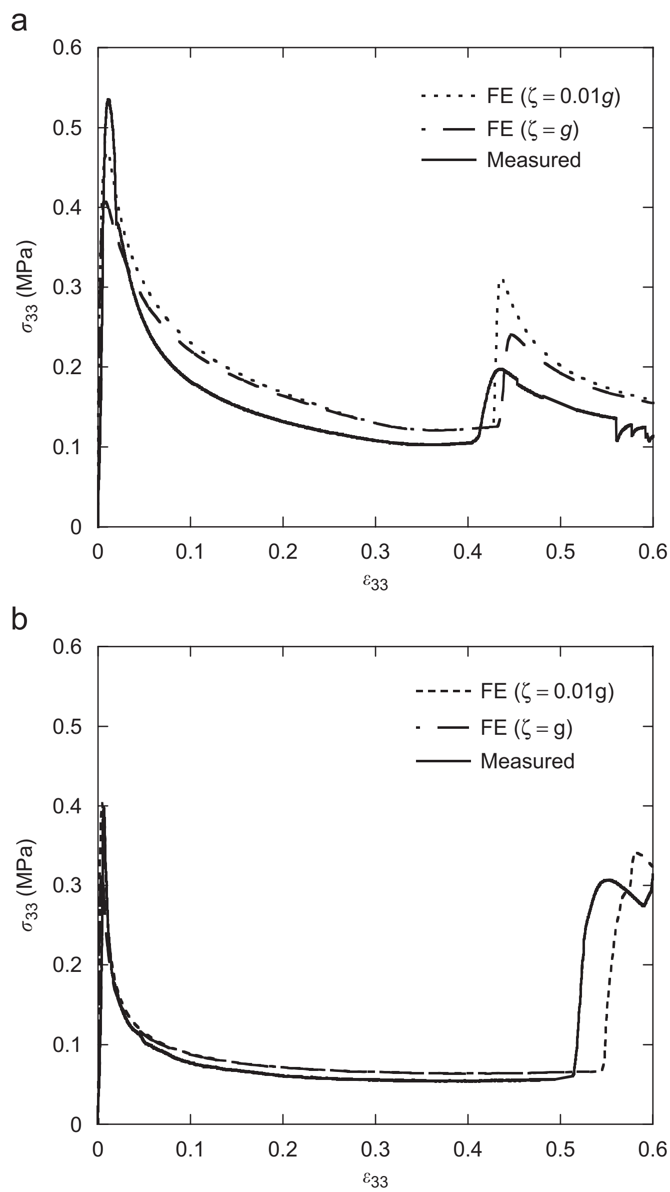

Fig. 5. The measured and predicted response of the compressive stress versus strain response of the Y-frame sandwich core. (a) No-sliding and (b) free-sliding boundary conditions.

the shear response of the Y-frame is expected to depend on the specimen length L. We conducted a series of longitudinal shear tests on specimens of length L in the range 45–300 mm (core thickness $c = 44$ mm in all cases). The measured peak shear strength τ_{13}^{p} (defined as the initial peak shear stress) is plotted as a function of the specimen aspect ratio L/c in Fig. 11. The peak shear strength is sensitive to specimen aspect ratio L/c for $L/c < 4$ but is reasonably constant at higher aspect ratios. This confirms that the results for $L/c \approx 7$, as plotted in Fig. 10a, are representative of those for a large specimen.

3.2.2. Transverse shear tests

Five Y-frames, each of length $L = 55$ mm, were assembled adjacent to each other along the x_2 direction

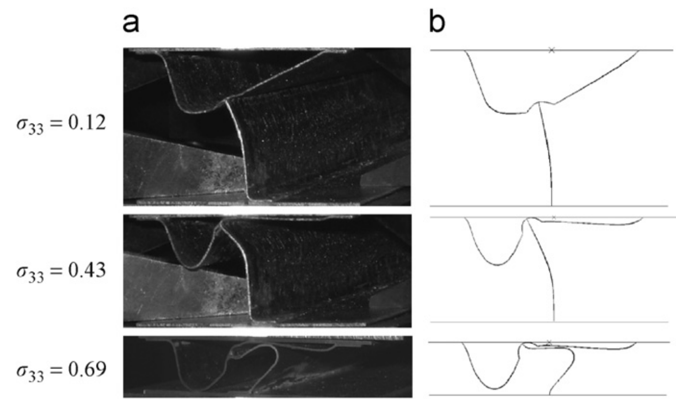

Fig. 6. (a) Observed shape and (b) FE prediction of the deformation mode of the Y-frame sandwich under uniaxial compression (no-sliding boundary condition). The deformed profiles are shown at three selected values of the nominal compressive strain ε_{33}.

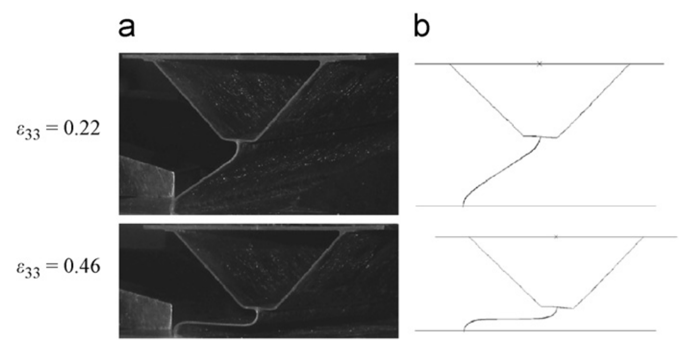

Fig. 7. (a) Observed and (b) FE prediction of the deformation mode of the Y-frame sandwich under uniaxial compression (free-sliding boundary condition). The deformed profiles are shown at two selected values of the nominal compressive strain ε_{33}.

and were brazed to face-sheets of thickness $t = 0.6$ mm. Sandwich beams of length $L = 300$ mm in the x_2 direction were thereby manufactured. A pair of specimens was used in each double-lap shear test, again using the apparatus sketched in Fig. 8. The transverse shear (τ_{23}–γ_{23}) response was measured using a similar procedure to that described above for the longitudinal shear tests.

This measured shear response τ_{23}–γ_{23} is plotted in Fig. 12. After an initial elastic response, the Y-frame sandwich core yields at a shear stress $\tau_{23}^{Y} \approx 0.03$ MPa and subsequently displays a mildly hardening response up to a shear strain $\gamma_{23} = 0.3$. Thereafter, the shear stress rises sharply with increasing shear strain. A photograph of the deformed specimen at an applied shear strain $\gamma_{23} = 0.3$ is shown in Fig. 13a. The low transverse shear strength of the Y-frame (compared to that in the longitudinal direction) is due to the formation of two plastic hinges in the Y-frame leg, one at the bottom and one at the joint between the leg and the upper half of the Y-frame. This mechanism results in only elastic deformation of the upper half of the Y-frame. It is argued that the sharp rise in shear stress for $\gamma_{23} > 0.3$ is due to the constraint by the double-lap shear apparatus upon normal straining in the x_3 direction.

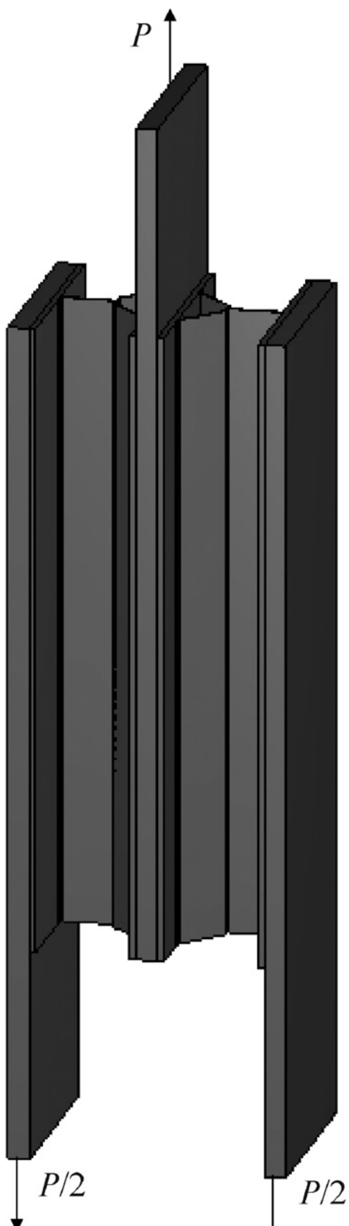

Fig. 8. Sketch of the double-lap shear rig used to test pair of Y-frame specimens in longitudinal and transverse shear. A Y-frame specimen loaded in longitudinal shear is shown here.

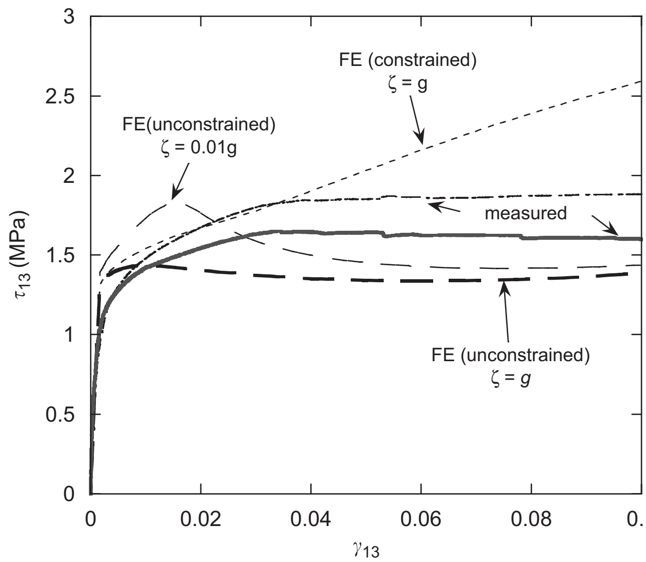

Fig. 9. The measured and predicted longitudinal shear response of the Y-frame sandwich core. Two separate measurements are plotted to indicate the variability in the measurements. FE predictions for the constrained and unconstrained boundary conditions are included for two selected values of imperfection.

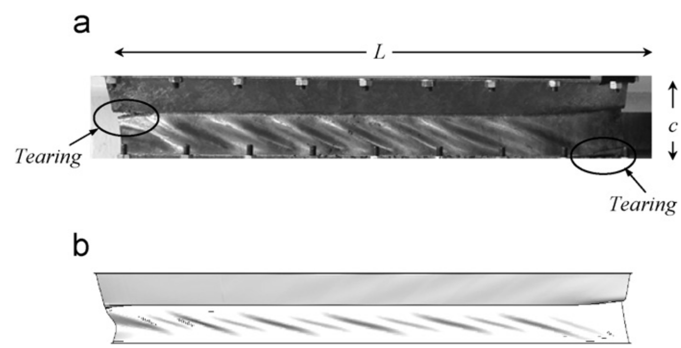

Fig. 10. (a) Observed and (b) predicted deformation mode of the Y-frame core under longitudinal shear. The deformed profiles are shown at a shear strain $\gamma_{13} = 0.1$.

At large shear strains the Y-frame leg stretches and consequently the applied shear stress increases sharply. Finite element calculations reported below clarify this effect.

3.3. Finite element predictions

Finite element calculations of the compressive and shear responses of the Y-frame sandwich core have been performed using the general finite element package ABAQUS (HKS—*Hibbitt, Karlsson & Sorensen, Inc.*). The geometry of the Y-frame analysed was identical to that employed in the experimental investigation (as detailed in Fig. 2). The FE model comprised about 25,000 linear shell elements (S4R in ABAQUS notation) of in-plane dimension $2g$, where g is the thickness of the sheet from which Y-frames were manufactured. A mesh sensitivity study revealed that additional mesh refinement did not change the results appreciably. All computations reported here employed such a mesh. The face-sheets were treated as rigid plates, and were modelled by the analytical rigid surface in ABAQUS. Possible contacts between any surfaces of the mesh were modelled by the hard, frictionless contact option in ABAQUS.

The stainless steel was treated as a rate-independent J2-flow theory solid with Young's modulus $E = 210\,\text{GPa}$ and Poisson ratio $\nu = 0.3$. The uniaxial tensile true stress versus equivalent plastic strain curve was tabulated in ABAQUS employing the measured data plotted in Fig. 3.

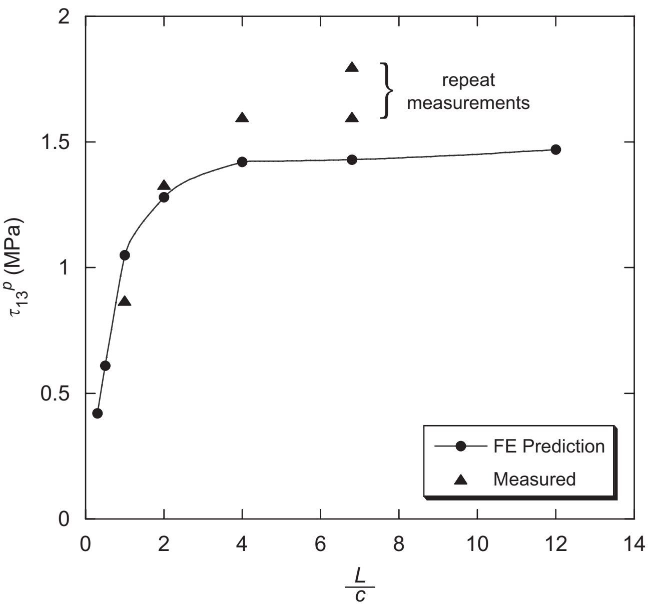

Fig. 11. A summary of the measured and FE predictions of the peak longitudinal shear strength of the Y-frame as a function of the specimen aspect ratio L/c.

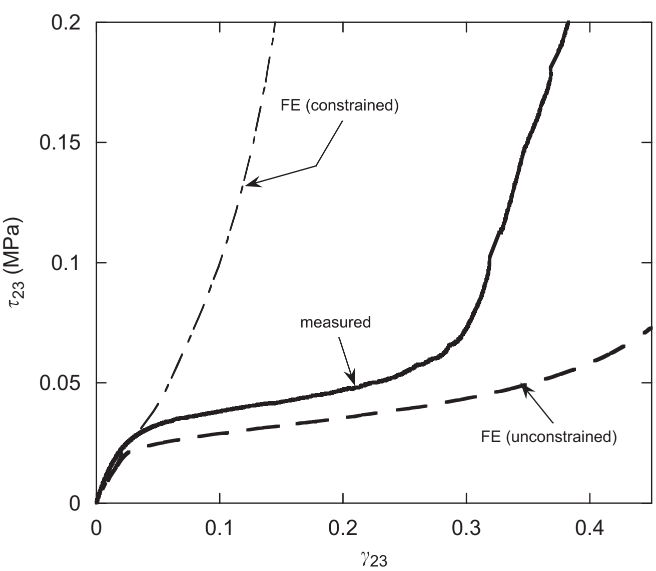

Fig. 12. The measured and predicted transverse shear response of the Y-frame sandwich core. FE predictions for both the constrained and unconstrained boundary conditions are given.

3.3.1. Compression simulations

The compression simulations were performed by imposing displacement boundary conditions. In both the free and no-sliding simulations, all degrees of freedom of the lower rigid plate were taken to be zero and a vertical compressive displacement rate (in the x_3 direction of Fig. 2b) was applied to the top plate (while constraining this top plate against any rotations). In the no-sliding simulations, the horizontal displacements of the top plate were also held at zero.

The compressive stress versus strain response was determined from the calculated force versus the applied vertical displacement. In order to trigger the appropriate collapse mode in the finite element simulations, an initial imperfection in the shape of the first elastic buckling eigenmode was introduced into the finite element model. Two levels of imperfection magnitude were considered in order to gauge the imperfection sensitivity of the compressive response of the Y-frame: $\zeta = 0.01g$ and $\zeta = g$, where ζ is the amplitude of the imperfection.

The predicted compression responses are compared with the observed behaviours in Figs. 5a and b for the no-sliding and free-sliding cases, respectively. Excellent agreement is noted. The finite element predictions of the compressive deformation mode in the no-sliding and free-sliding cases are included in Figs. 6 and 7, respectively. Again, the finite element calculations capture the observed deformation modes to good accuracy. It is noted in passing that the peak compressive strength of the Y-frame sandwich core involves plastic collapse of the stainless steel. Exploratory finite element calculations were performed with the stainless steel modelled as a linear elastic solid: much higher peak strengths were obtained in these calculations.

3.3.2. Longitudinal shear simulations

Finite element simulations of the longitudinal shear response of the Y-frame sandwich core were conducted with two sets of boundary conditions in order to simulate the possible constraints imposed by the double-lap shear apparatus. Loading in the longitudinal direction was applied by prescribing a displacement in the x_1 direction to the top face-sheet while the bottom face-sheet (attached to the Y-frame leg) was held motionless. Two choices of constraint in the out-of-plane x_3 direction were assumed: *unconstrained* simulations where the traction T_3 on the top face-sheet vanishes, and *constrained* simulations where the displacements u_3 on the top face-sheet vanishes. These two choices of boundary conditions bound the constraint imposed by the double-lap shear apparatus.

An initial imperfection is introduced into the FE model in order to trigger the appropriate collapse mode. In line with the experimental observations of the deformation mode (Fig. 10a) an elastic buckling eigenmode, with wrinkles within the Y-frame leg and negligible deformation in the upper half of the Y-frame, was chosen to model the imperfections in the Y-frame. This mode was the seventh lowest mode of an eigenvalue analysis. Maximum imperfection magnitudes of $\zeta = 0.01g$ and g were chosen in order to explore the imperfection sensitivity of the Y-frame response.

A comparison between the predicted $\tau_{13}-\gamma_{13}$ response and the observed behaviour is presented in Fig. 9 for the choice $L/c = 7$. Consider first the *unconstrained* simulations. A pronounced peak in shear stress is observed at $\gamma_{13} \approx 0.01$ for a small imperfection, $\zeta = 0.01g$, while the shear stress increases monotonically with increasing shear strain when a large imperfection is present, $\zeta = g$. The predicted shear stress at large shear strain $\gamma_{13} > 0.04$ is relatively insensitive to the level of imperfection and to the

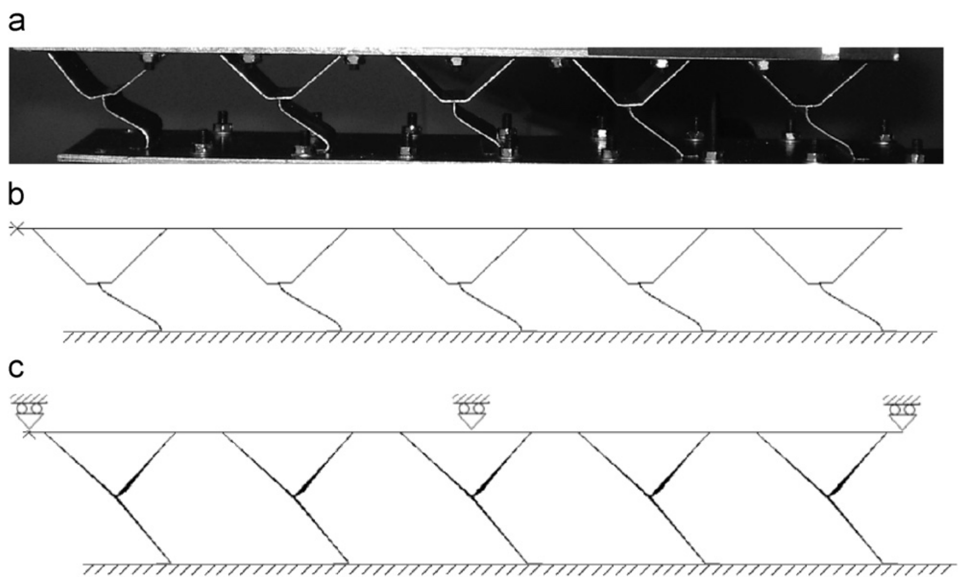

Fig. 13. (a) Observed shape, (b) predicted shape for unconstrained boundary condition and (c) predicted shape for constrained boundary condition, of the Y-frame core subject to transverse shear. The deformed profiles are shown at a shear strain $\gamma_{23} = 0.3$.

degree of straining. The observed response resembles that of the unconstrained simulation at large imperfection, with the measured plateau strength somewhat above the prediction.

Second, consider the constrained FE simulations. An approximately linear hardening response is predicted beyond the elastic limit. Negligible sensitivity to the imperfection magnitude is observed and hence only the $\zeta = g$ results are plotted in Fig. 9. We conclude that the constraint imposed by the double-lap shear apparatus is intermediate between the two limiting sets of boundary conditions considered here. The predicted deformed mode in shear is shown in Fig. 10b alongside the experimental photograph at $\gamma_{13} = 0.10$. The FE model predicts correctly that wrinkling occurs in the Y-frame leg, with the upper half of the Y-frame undergoing only elastic deformation.

A comparison between the measurements and FE predictions (unconstrained) of the longitudinal peak shear strength τ_{13}^{p} of the Y-frame is shown in Fig. 11 as a function of the Y-frame aspect ratio L/c. Consistent with the results in Fig. 9, the unconstrained FE calculations slightly under-predict the longitudinal shear flow strength over the range of aspect ratios investigated here. Both measurement and analysis reveal that the longitudinal shear flow strength plateaus out for $L/c \geqslant 4$.

3.3.3. *Transverse shear simulations*

Finite element simulations of the transverse shear response of the Y-frame were performed by considering the test geometry of five Y-frame sections, as shown in Fig. 13. The spacing between the Y-frames matched that of the experiments. Again, rigid face-sheets were tied to the Y-frame and hard frictionless contact was modelled between all surfaces. Loading was applied by prescribing a displacement in the x_2 direction to the top face-sheet while the bottom face-sheet was fully constrained. *Unconstrained* and *constrained* simulations were performed as for the longitudinal shear case: the displacements $u_3 = 0$ were specified on the top face-sheet in the constrained case whereas the traction T_3 was fully relaxed in the unconstrained case. An imperfection in the form of the first elastic buckling eigenmode was introduced into the FE model: in this orientation, the FE predictions of the shear response are insensitive to the magnitude of the imperfection within the range $\zeta = 0.01g$–g. Thus, for the sake of brevity, only results for $\zeta = g$ are presented below.

Comparisons between the measurements and FE predictions of the transverse shear response τ_{23}–γ_{23} are shown in Fig. 12. The unconstrained boundary condition adequately predicts the measurements for $\gamma_{23} < 0.3$, but at higher strain levels it does not capture the stiffening imposed by the double-lap shear apparatus. In contrast, the constrained FE calculations predict a much stronger response than the measurements over the full range of shear strains investigated here. However, the slope $d\tau_{23}/d\gamma_{23}$ of the measured response is similar to the constrained FE predictions for $\gamma_{23} > 0.3$. This suggests that the constrained boundary conditions are more appropriate to model the experiments at large levels of shear strain.

4. Indentation of Y-frame sandwich beams

We proceed to investigate the transverse indentation response of Y-frame sandwich beams on a rigid foundation. The problem under consideration is sketched in Fig. 14. The beams were of length $L = 600$ mm along the x_1 direction and were indented in the x_3 direction. Each beam was constructed from two adjacent Y-frame sections in the

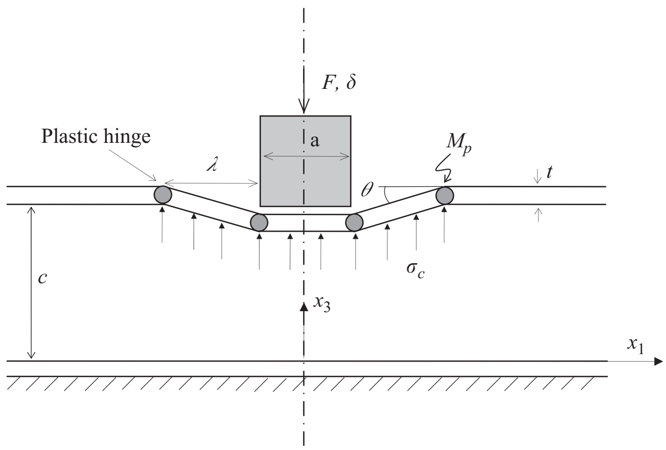

Fig. 14. The assumed deformation mode for indentation of the Y-frame sandwich. The Y-frame sandwich is indented by a flat bottom punch of width a and rests on a rigid foundation.

x_2 direction, giving a width of $b = 115$ mm. Stainless steel face-sheets were used, of thickness $t = 0.6$ mm and 1.2 m. The indentation response was determined for the following mild steel indenters:

(i) a flat bottomed punch of width $a = 5$ mm,
(ii) a flat bottomed punch of width $a = 15$ mm and
(iii) a circular roller of radius $R = 9$ mm.

The indenters were of length 140 mm along the x_2 direction in order to ensure a uniform indentation over the entire 115 mm width of the beam.

The indentation experiments were performed in a screw-driven test machine at an indentation rate $\dot{\delta} = 0.3\,\mathrm{mm}\,min^{-1}$ and the indentation force F was measured via the load cell of the test machine. The relative displacement δ of the top and bottom face-sheets of the Y-frame sandwich directly beneath the indenter was measured using a laser extensometer.

The measured normalised load $\bar{F} \equiv F/(\sigma_Y bt)$ versus normalised indentation depth $\bar{\delta} \equiv \delta/c$ response of the Y-frame sandwich beams are plotted in Fig. 15a and b for the $R = 9$ mm radius roller and the $a = 15$ mm wide flat bottom punch, respectively. In the normalisation of load, use is made of the measured yield strength of the as-brazed 304 stainless steel from which the Y-frame sandwich beams are constructed, $\sigma_Y = 210$ MPa. Results are presented for both choices of face-sheet thickness, $t = 0.6$ and 1.2 mm.

In all cases, the indentation response has an initial elastic regime followed by a plateau regime where the indentation force remains approximately constant with increasing indentation depth. The normalised indentation forces for the sandwich beams with thicker face-sheets ($t = 1.2$ mm) are lower than those for the sandwich beams with the $t = 0.6$ mm face-sheets. A comparison between the observed deformation modes at an indentation depth $\delta = 10$ mm is shown in Fig. 16 for the indentation of the $t = 0.6$ mm beams by the three types of indenters

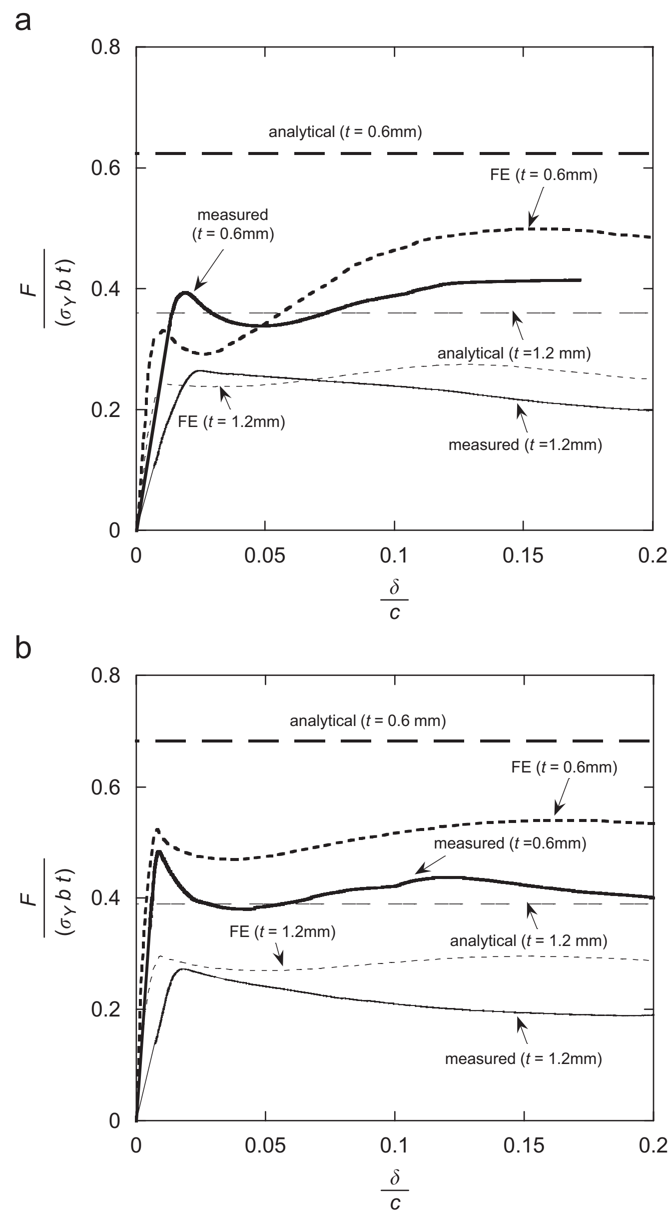

Fig. 15. The measured non-dimensional indentation load versus indentation depth of the Y-frame sandwich indented by (a) a roller of radius $R = 9$ mm and (b) a flat bottom indenter of width $a = 15$ mm. The measured responses for sandwiches with face-sheet thicknesses $t = 0.6$ and 1.2 mm are included along with the corresponding FE and analytical predictions.

described above. The sandwich deformation involves core compression, core shear and face-sheet stretching in all cases.

The measured values of peak load and plateau load (defined as the average indentation load between indentation depths $0.1 \leqslant \delta/c \leqslant 0.15$) are listed in Tables 1 and 2, respectively. Results are given for the three indenter geometries and for sandwich beams of face-sheet thickness $t = 0.6$ and 1.2 mm. Analytical and FE predictions are now reported and are compared with these measurements.

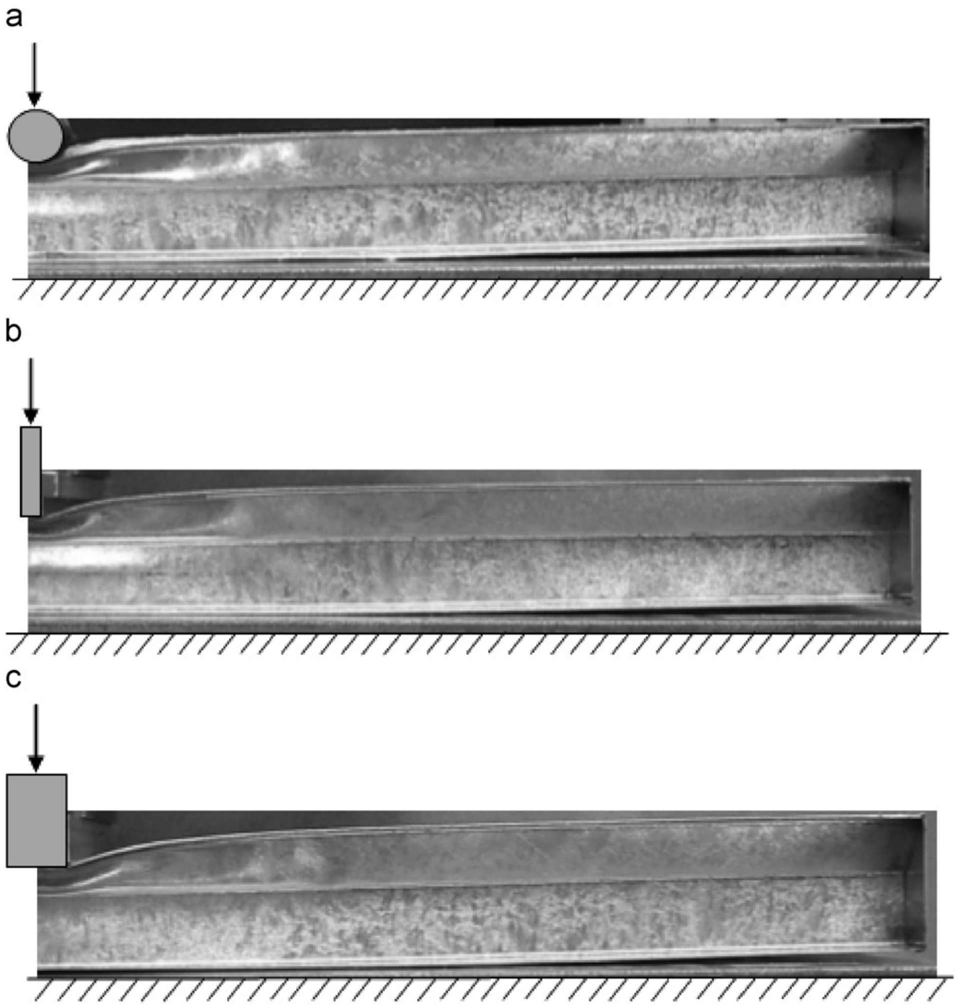

Fig. 16. The observed deformation modes of the $t = 0.6$ mm Y-frame sandwich indented by (a) the $R = 9$ mm roller, (b) the $a = 10$ mm flat bottom indenter and (c) the $a = 15$ mm wide flat bottom indenter. The deformed profiles are shown at an indentation depth $\delta = 10$ mm.

Table 1
A comparison between the measured, analytical predictions and FE predictions of the normalised peak indentation loads of all the sandwich beams tested in this study

Face-sheet thickness (mm)	Indenter dimensions (mm)	Non-dimensional peak load, $F_{peak}/\sigma_Y bt$			
		Analytical prediction		FE	Experiment
		$\tau^p_{13} = 0$	$\tau^p_{13} = 1.7$ MPa		
$t = 0.6$	Roller $R = 9$	0.10	0.69	0.33	0.39
	Flat bottom $a = 5$	0.12	0.7	0.42	0.44
	Flat bottom $a = 15$	0.16	0.75	0.52	0.48
$t = 1.2$	Roller $R = 9$	0.10	0.39	0.24	0.26
	Flat bottom $a = 5$	0.11	0.4	0.26	0.27
	Flat bottom $a = 15$	0.13	0.42	0.29	0.27

4.1. Analytical predictions

Ashby et al. [8] have presented an analytical model for the indentation of sandwich beams comprising metal foam cores. The contribution of the shear strength of the foam to the indentation load was neglected and only the contributions from compression of the core and from bending of the face-sheets were considered. We have already observed in the present study that the longitudinal shear strength of the Y-frame considerably exceeds the compressive strength

Table 2
A comparison between the measured and FE predictions of the normalised plateau indentation loads of all the sandwich beams tested in this study

Face-sheet thickness (mm)	Indenter dimensions (mm)	Plateau loads, $F_{ss}/\sigma_Y bt$	
		FE	Experiment
$t = 0.6$	Roller $R = 9$	0.49	0.41
	Flat bottom $a = 5$	0.52	0.40
	Flat bottom $a = 15$	0.53	0.43
$t = 1.2$	Roller $R = 9$	0.27	0.23
	Flat bottom $a = 5$	0.28	0.23
	Flat bottom $a = 15$	0.29	0.20

The plateau indentation load F_{ss} is defined as the average indentation load for indentation depths in the range $0.1 \leqslant \delta/c \leqslant 0.15$.

(see Section 3) and we anticipate that the high shear strength of the core contributes to the indentation strength. An analytical model is now derived for the peak indentation force of the Y-frame sandwich beam resting upon a rigid foundation. We emphasise that the aim of this analysis is not to provide an accurate estimate of the measurements but rather (i) to act as an *upper bound* on the indentation loads with the analysis of Ashby et al. [8] serving as a lower bound and (ii) demonstrate the influence of the shear strength of the core on the indentation strength of sandwich beams.

The Y-frame core and face-sheets are idealised as homogenous rigid, ideally plastic solids. The face-sheets are assumed to have a tensile strength σ_Y while the Y-frame has a compressive strength σ_{33}^p in the x_3 direction and a longitudinal shear strength τ_{13}^p. Assume that the Y-frame can compress in the x_3 direction without straining along the x_1 direction, and assume that the shear and compressive strengths of the Y-frame are decoupled. Consider the collapse mode as sketched in Fig. 14 and employ the co-ordinate system shown in Fig. 14. Then, the deformation mode is written as

$$u(x_1, x_3) = 0, \tag{1a}$$

$$v(x_1, x_3) = \begin{cases} \frac{\dot{\theta}}{c}\left(\lambda + \frac{a}{2} - x_1\right)x_3, & \frac{a}{2} \leqslant x_1 \leqslant \frac{a}{2} + \lambda, \\ \frac{\dot{\theta}}{c}\lambda x_3, & -\frac{a}{2} \leqslant x_1 \leqslant \frac{a}{2}, \\ \frac{\dot{\theta}}{c}\left(\lambda + \frac{a}{2} + x_1\right)x_3, & -\frac{a}{2} - \lambda \leqslant x_1 \leqslant -\frac{a}{2}, \end{cases} \tag{1b}$$

where a is the width of the indenter. Here, u and v are displacements in the x_1 and x_3 directions, respectively, c is the core thickness and λ is the length of the small segments of the top face-sheet that rotate through an angle θ. The collapse load F (per unit depth in the x_2 direction) can be derived by a simple upper bound calculation as

$$F\lambda\theta = 4M_P\theta + \int_A \sigma_{33}^p \varepsilon_{33}\,\mathrm{d}A + \int_A \tau_{13}^p \gamma_{13}\,\mathrm{d}A, \tag{2}$$

where the usual strain components are $\varepsilon_{33} = \partial v/\partial x_3$ and $\gamma_{13} = \partial v/\partial x_1 + \partial u/\partial x_3$. The integrals in Eq. (2) are over the rectangular region $-\frac{a}{2} - \lambda \leqslant x_1 \leqslant \frac{a}{2} + \lambda$ and $0 \leqslant x_3 \leqslant c$ while the plastic bending moment of the face-sheets of thickness t is given by $M_P \equiv \sigma_Y t^2/4$. This expression for the indentation force reduces to

$$F = \frac{\sigma_Y t^2}{\lambda} + \sigma_{33}^p(\lambda + a) + \tau_{13}^p c. \tag{3}$$

Now, minimise this upper bound solution for F with respect to the free parameter λ to obtain the indentation load F_I, where

$$F_I = 2t\sqrt{\sigma_Y \sigma_{33}^p} + \sigma_{33}^p a + \tau_{13}^p c, \tag{4}$$

and the length λ is

$$\lambda = t\sqrt{\frac{\sigma_Y}{\sigma_{33}^p}}. \tag{5}$$

We proceed to compare the prediction (4) with the measured indentation load. Unless otherwise specified, in these comparisons we take the tensile yield strength of the face-sheet material to be $\sigma_Y = 210\,\mathrm{MPa}$ (Fig. 3), the peak compressive strength of the Y-frame as $\sigma_{33}^p = 0.5\,\mathrm{MPa}$ (Fig. 5) and the longitudinal shear strength as that of the $L/c = 7$ specimen, i.e. $\tau_{13}^p = 1.7\,\mathrm{MPa}$ (Fig. 9). Comparisons between the measurements and the analytical predictions of the indentation load are given in Fig. 15a and b for indentation by the $R = 9\,\mathrm{mm}$ roller and by the flat bottom indenter of width $a = 15\,\mathrm{mm}$, respectively. (For the roller we take $a = 0$ in Eq. (4).) The analytical predictions overestimate the measurements of the peak loads substantially. We attribute this discrepancy to the fact that the Y-frame core does not deform in a homogeneous manner. Eq. (4) provides an upper bound to the indentation load and it may be significantly higher than the true collapse load.

The analytical predictions of the normalised peak indentation load with $\tau_{13}^p = 1.7\,\mathrm{MPa}$ and $\tau_{13}^p = 0$ are included in Table 1. In similar manner to the comparisons shown in Fig. 15, the analytical predictions with $\tau_{13}^p = 1.7\,\mathrm{MPa}$ overestimate the measured loads in all cases. We attribute this discrepancy to the fact that the homogenised response of the Y-frame assumed in the analytical model is inappropriate: the large gradients in strain across the core make it important to take the structural features of the Y-frame into account as will be shown in the FE analysis presented subsequently. On the other hand, a neglect of the shear strength in the analytical model ($\tau_{13}^c = 0$) leads to a significant under-prediction of the indentation strength. This confirms our initial hypothesis that the shear strength of the Y-frame core plays an important role in dictating the indentation strength of the Y-frame beams.

4.2. Finite element predictions

Finite element calculations of the indentation response of the Y-frame core sandwich beams have been performed using the finite element package ABAQUS. The geometry of the beams was identical to that used in the experimental investigation (cross-sectional dimensions detailed in Fig. 2) and both the face-sheets and the Y-frame core were modelled using linear shell elements (S4R in ABAQUS notation) with a mesh size of $2g$ as in Section 3.3. The face-sheets were tied to the top half and leg of the Y-frame and contact between the surfaces were modelled using the hard, frictionless contact option in ABAQUS. The imposed boundary conditions were as follows. All degrees of freedom (rotational and translational) of all nodes on the bottom face-sheet were held at zero in order to simulate sticking friction between the rigid foundation and the bottom face-sheet of the Y-frame core sandwich. Rigid indenters, of geometry matching those employed in the experiments, indented the beam by imposing an increasing displacement. Contact between the outer surface of the top face-sheet and the rigid indenters was modelled using the frictionless contact option as provided by ABAQUS. The material properties of the Y-frame core sandwich sheets was taken to be the same as those used in the simulations described in Section 3.3.

Comparisons between the predicted and measured indentation load versus displacement response are shown in Fig. 15a and b for indentation with the $R = 9$ mm diameter roller and the $a = 15$ mm flat bottom punch, respectively. Reasonable agreement is observed. A more complete comparison is given in Tables 1 and 2 where the measured values of the peak load and plateau load are compared with the FE predictions. The agreement between FE predictions and measurements is within 8% in all cases.

4.3. A comparison of Y-frame sandwich beams with metal foam core sandwich beams of equal mass

Metal foam core sandwich beams have been developed for lightweight structural and energy absorption applications, see for example Ashby et al. [8]. Here, we compare the FE predictions of the indentation response of sandwich beams containing a Y-frame or a metal foam core of equal mass.

Two metal foam core sandwich beams with 304 stainless steel face-sheets of thickness $t = 0.6$ and 1.2 mm are considered. These beams have the same overall geometry as the Y-frame beams described above, i.e. length $L = 600$ mm, width $b = 115$ mm and core thickness $c = 44$ mm. For the sake of brevity only the indentation of the metal foam core beams by the $R = 9$ mm rigid roller is addressed here. Plane strain FE calculations were performed using ABAQUS, with both the foam core and face-sheets modelled using four-noded plane strain elements (CPE4 in ABAQUS notation). The face-sheets were modelled as J2 flow theory solids as for the Y-frame beams while the Deshpande and Fleck [9] model was used to describe the constitutive response of the metal foam core. Write s_{ij} as the usual deviatoric stress and the von Mises effective stress as $\sigma_e \equiv \sqrt{3s_{ij}s_{ij}/2}$. Then, the isotropic yield surface for the metal foam is specified by

$$\hat{\sigma} - Y = 0, \tag{6}$$

where the equivalent stress $\hat{\sigma}$ is a homogeneous function of σ_e and mean stress $\sigma_m \equiv \sigma_{kk}/3$ according to

$$\hat{\sigma}^2 \equiv \frac{1}{1 + (\alpha/3)^2}[\sigma_e^2 + \alpha^2\sigma_m^2]. \tag{7}$$

The material parameter α denotes the ratio of deviatoric strength to hydrostatic strength, and the normalisation factor on the right hand side of relation (7) is chosen such that $\hat{\sigma}$ denotes the stress in a uniaxial tension or compression test. Normality of plastic flow is assumed, and this implies that the "plastic Poisson's ratio" $v_p = -\dot{\varepsilon}_{22}^p/\dot{\varepsilon}_{11}^p$ for uniaxial compression in the one-direction is given by

$$v_p = \frac{1/2 - (\alpha/3)^2}{1 + (\alpha/3)^2}. \tag{8}$$

In order to make a direct comparison with the stainless steel Y-frame sandwich core beams, we consider a metal foam with a relative density $\bar{\rho} = 0.02$ and made from stainless steel of yield strength $\sigma_Y = 210$ MPa. Thus, the core has the same overall size and mass as that of the Y-frame core. Following Ashby et al. [8], we specify that this foam has a Young's modulus $E_c = 1$ GPa, elastic Poisson's ratio $v = 0.3$ and a plastic Poisson's ratio $v_P = 0$. The uniaxial compressive stress versus plastic strain response is assumed to be given by

$$Y = \begin{cases} 0.3\bar{\rho}^{1.5}\sigma_Y, & \hat{\varepsilon}^P \leqslant \varepsilon_D, \\ 0.3\bar{\rho}^{1.5}\sigma_Y + E_c(\hat{\varepsilon}^P - \varepsilon_D), & \text{otherwise}, \end{cases} \tag{9}$$

where $\dot{\hat{\varepsilon}}^p$ is the plastic strain rate that is work conjugate to $\hat{\sigma}$ and $\varepsilon_D \equiv -\ln(\bar{\rho})$ is the logarithmic densification strain beyond which negligible plastic straining of the foam occurs. Thus, the compressive plateau strength of the metal foam core is $Y(\hat{\varepsilon}^p \leqslant \varepsilon_D) \approx 0.2$ MPa.

The boundary conditions were specified as follows. All degrees of freedom of all nodes on the bottom face-sheet were completely constrained in order to simulate sticking friction between the rigid foundation and the bottom face-sheet of the metal foam core sandwich. Loading was applied through prescribed displacements of rigid $R = 9$ mm roller. And contact between the outer surface of the top face-sheet and the rigid indenter were modelled by frictionless contact as provided by ABAQUS.

The normalised indentation force $\bar{F} \equiv F/(\sigma_Y bt)$ versus normalised displacement $\bar{\delta} \equiv \delta/c$ response of the metal foam sandwich beams with face-sheets are plotted in Fig. 17a along with the corresponding predictions for the Y-frame sandwich from Fig. 15. Results are shown for the two face-sheet thicknesses, $t = 0.6$ and 1.2 mm. In contrast to the response of the Y-frame sandwich, the metal foam core sandwich beam displays a monotonically increasing indentation force with increasing indentation depth. At any given indentation depth, the indentation force for the Y-frame sandwich beams is significantly higher than that of

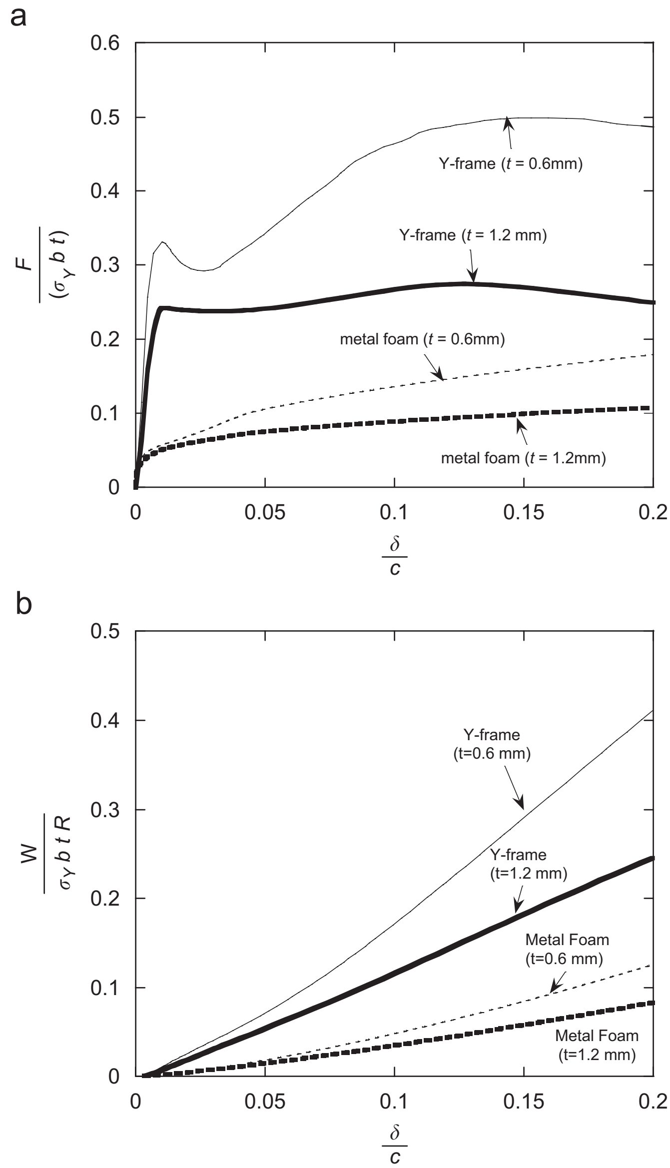

Fig. 17. A comparison between the normalised (a) indentation load versus indentation depth and (b) energy absorption versus indention depth responses of the Y-frame and metal foam sandwich core beams. The sandwich beams have 304 stainless steel face-sheets of thickness $t = 0.6$ and 1.2 mm. The metal foam core is made from stainless steel and has a relative density equal to that of the Y-frame core.

the corresponding metal foam core beam. The energy absorption W of the sandwich beams is defined as

$$W(\delta) = \int_0^{\delta} F \, d\delta, \tag{10}$$

with the normalised energy absorption $\bar{W} \equiv W/(\sigma_Y bRt)$. This normalised energy absorption is plotted against the normalised indentation depth $\bar{\delta}$ for the metal foam and Y-frame sandwich beams in Fig. 17b. As expected, the Y-frame sandwich beams significantly outperform their metal foam counterparts in that that they absorb more energy for any given indentation depth.

In the above comparison, it is clear that the Y-frame sandwich beams outperform the equivalent metal foam core beams. However, the possibility of face-sheet tearing has been neglected in the comparison. In most practical circumstances failure of the beam is dictated by tearing of the face-sheets rather than by a limiting indentation depth. It is instructive to cross-plot the normalised energy absorption $\bar{W}$ against the maximum principal strain ε_{max} in the face-sheets in order to determine which beam absorbs more energy prior to the initiation of tearing in the face-sheets, as characterised by the ε_{max}. The FE predictions of $\bar{W}$ versus ε_{max} for the $t = 0.6$ and 1.2 mm Y-frame core and metal foam core sandwich beams are shown in Fig. 18a. These curves are determined as follows. For a given indentation depth δ, the energy absorption $\bar{W}$ is determined via Eq. (10) while ε_{max} determined by examining the through-thickness average strains in the face-sheets. These two values give one point on the $\bar{W}$ versus ε_{max} curve in Fig. 18a. This procedure has been repeated for a large number of values of δ in order to construct the curves shown in Fig. 18a. The trajectories plotted in Fig. 18a are limited to the regime $\bar{\delta} < 0.2$, consistent with the data presented in Fig. 17.

It is concluded from Fig. 18a that the metal foam core provides for a larger value of absorbed energy $\bar{W}$ than the Y-frame, for any assumed value of ε_{max}. The strain concentrations for the foam core and the Y-frame are compared in Fig. 18b and c, respectively. Severe strain concentrations are present at the joints of the Y-frame, and these lead to its reduced energy absorption capacity. An alternative approach is to assume that the maximum face-sheet strain dictates the limiting strain for both types of core. When this assumption is made, the energy absorption capacities of the Y-frame and metal foam core sandwich beams are similar.

5. Concluding remarks

Y-frame sandwich beams made from AISI type 304 stainless steel sheets have been manufactured by a folding, slotting and brazing technique. The out-of-plane compressive and transverse shear responses are governed by plastic bending of the constituent struts of the Y-frame. Under longitudinal shear the Y-frame leg undergoes uniform straining prior to the onset of plastic wrinkling. Thus, the Y-frame has a low compressive and transverse shear strength but a high longitudinal shear strength. These measured compressive and shear responses of the Y-frame sandwich core are in good agreement with three-dimensional finite element predictions.

The Y-frame sandwich beams are designed to withstand low velocity impacts by spreading the load over a large area and thus preventing the tearing of the sandwich beam face-sheets. In this study, we have investigated the transverse indentation response of Y-frame sandwich beams resting upon a rigid foundation. The high longitudinal shear strength of the Y-frame increases the indentation strength of the Y-frame beams substantially: while an analytical upper bound analysis for this indentation process over-predicts the indentation strength, the

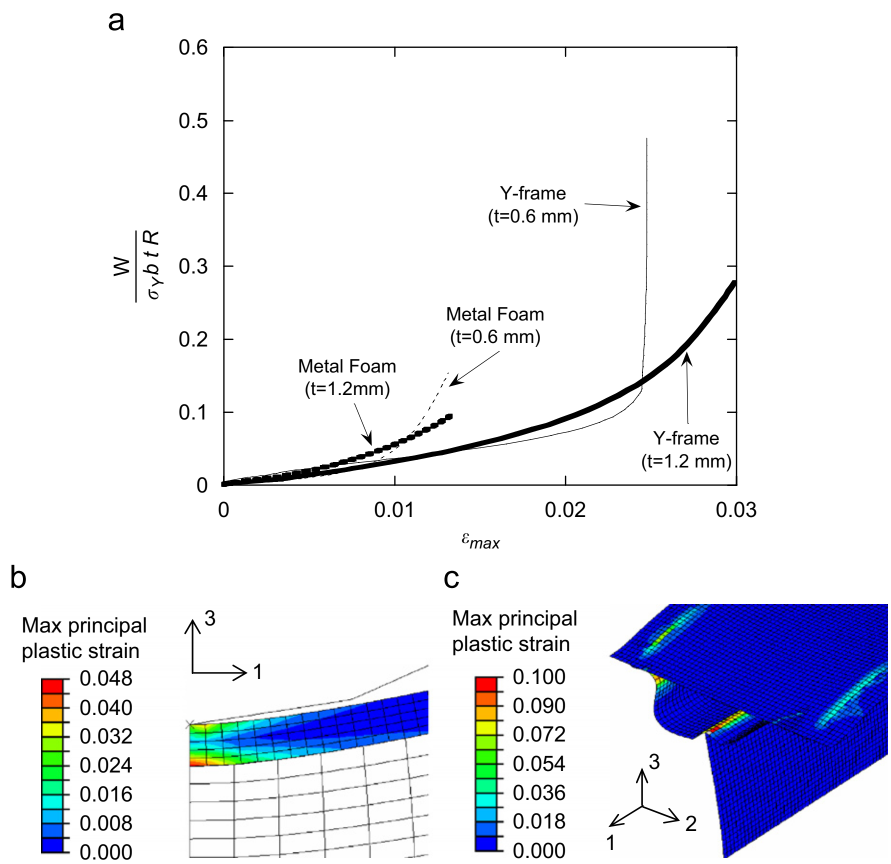

Fig. 18. (a) The normalised energy absorption versus maximum principal strain in the face-sheets of the Y-frame and metal foam core sandwich beams considered in Fig. 16. The deformed profiles of sandwich beams with $t = 0.6$ mm face-sheets at an indentation depth $\delta = 10$ mm are shown (b) for the metal foam core and (c) for the Y-frame core. Contours of maximum principal strain are included in these deformed profiles.

three-dimensional finite element simulations capture the response to a high level of accuracy. These finite element simulations demonstrate that for any given indentation depth, the Y-frame sandwich beams absorb significantly more energy than metal foam core sandwich beams of equal mass. However, the Y-frame induces large strain concentrations in the top face-sheet that increases the likelihood of tearing of the face-sheet.

Acknowledgments

This work was supported by the Netherlands Institute for Metal Research, project no. MC1.03163, *The Optimal Design of Y-core sandwich structures*.

References

[1] Deshpande VS, Fleck NA. Collapse of truss core sandwich beams in 3-point bending. International Journal of Solids and Structures 2001; 38(36–37):6275–305.

[2] Paik JK. Innovative structural designs of tankers against ship collisions and grounding: a recent state-of-the-art review. Marine Technology 2003;40(1):25–33.

[3] Wevers LJ, Vredeveldt AW. Full scale ship collision experiments 1998. TNO-report 98-CMC-R1725. The Netherlands, 1999.

[4] Ludolphy, H. The unsinkable ship—development of the Y-shape support web. In: Proceedings of the 2nd international conference on collision and grounding of ships, Copenhagen, Denmark, 2001.

[5] Konter A, Broekhuijsen J, Vredeveldt A. A quantitative assessment of the factors contributing to the accuracy of ship collision predictions with the finite element method. Tokyo, Japan: International Conference of Ship Collisions and Grounding; 2004.

[6] Naar H, Kujala P, Simonsen BC, Ludolphy H. Comparison of the crashworthiness of various bottom and side structures. Marine Structures 2002;15(4–5):443–60.

[7] Pedersen CBW, Deshpande VS, Fleck NA. Compressive response of the Y-shaped sandwich core. European Journal of Mechanics—A/Solids 2004;25:125–41.

[8] Ashby M, Evans A, Fleck N, Gibson L, Wadley H. Metal foams: a design guide. Butterworth Heinemann; 2000.

[9] Deshpande VS, Fleck NA. Isotropic constitutive models for metallic foams. Journal of Mechanics and Physics of Solids 2000;48(6–7): 1253–83.